PROCEEDINGS OF SPIE

SPIEDigitalLibrary.org/conference-proceedings-of-spie

Photodetector fabrication by dielectrophoretic assembly of GaAs nanowires grown by a two-steps method

Carlos García Núñez, Alejandro F. Braña, Nair López, José L. Pau, Basilio J. García

SPIE.

Downloaded From: https://www.spiedigitallibrary.org/conference-proceedings-of-spie on 10/26/2017 Terms of Use: https://spiedigitallibrary.spie.org/ss/TermsOfUse.aspx

Invited Paper

Photodetector fabrication by dielectrophoretic assembly of GaAs nanowires grown by a two-steps method

*Carlos García Núñez†, Alejandro F. Braña, Nair López, José L. Pau, Basilio J. García**

Grupo de Electrónica y Semiconductores, Dpto. de Física Aplicada, Facultad de Ciencias, Universidad Autónoma de Madrid, 28049 Madrid, Spain

† Currently at: Bendable Electronics and Sensing Technologies, Electronics and Nanoscale Engineering, University of Glasgow, G128QQ Glasgow, United Kingdom.

ABSTRACT

GaAs nanowires (NWs) are promising advanced materials for the development of high performance photodetectors in the visible and infrared range. In this work, we optimize the epitaxial growth of GaAs NWs compared to conventional procedures, by introducing a novel two-steps growth method that exhibits an improvement of the resulting NW aspect-ratio and an enhancement of the NW growth rate. Moreover, we investigate the contactless manipulation of NWs using non-uniform electric fields to assemble a single GaAs NW on conductive electrodes, resulting in assembly yields above 90%/site and an alignment yields of around 95%. The electrical characteristics of the dielectrophoretic contact formed between the NW and the electrode have been measured, observing that the use of n-type Al-doped ZnO (AZO) as electrode material for NW alignment produces Schottky barrier contacts with the GaAs NW body. Moreover, our results show the fast fabrication of diodes with rectifying characteristics due to the formation of a low-resistance contact between the Ga catalytic droplet at the tip of the NW and the AZO electrode. The current-voltage measurements of a single GaAs NW diode under different illumination conditions show a strong light responsivity of the forward bias characteristic mainly produced by a change on the series resistance.

Keywords: semiconductor nanowire, photodetector, dielectrophoresis, chemical beam epitaxy

1. INTRODUCTION

Semiconducting nanowires (NWs) are promising building blocks for the development of advanced electronics, optoelectronics, photonics, photovoltaics, sensing, etc. due to well-known properties such as their high surface-to-volume ratio, low dimensionality and high crystal quality. These NWs are therefore attractive candidates to improve existing technology based on thin films and bulk materials. In particular, III-V NWs are expected to play a crucial role for the development of a wide number of high-performance applications, including solar cells [1], photodetectors [2], resonant tunneling diodes [3], single electron transistors [4], and single photon emitters [5], mainly due to properties such as direct bandgaps, high carrier mobility, and the possibility to integrate these NWs directly in Si technology. However, while significant advances have been made on the characterization of NWs, their controlled growth and accurate manipulation/placement over conventional and non-conventional substrates are still considerable challenges, hindering to manufacture large-scale complex systems.

The growth of NWs through a bottom-up approach is typically carried out by metal-assisted vapor-liquid-solid (VLS) mechanism, using a metallic particle to assist the growth of the NW along a preferential direction fixed by the orientation of the crystalline substrate [6]. Vertically aligned GaAs NWs have been grown on Si substrates by different techniques such as molecular beam epitaxy (MBE) [7,8], and chemical beam epitaxy (CBE) [9,10], typically using Au and Ga as seed particles mainly due to the possibility to form a supersaturated liquid alloy with growth species. Although Au has been extensively used in GaAs NW growths, it could be unintentionally incorporated into the NW structure [11], and leads to form zincblende/wurtzite (ZB/WZ) polytypisms along the NW, which are important drawbacks that justify a wider use of Ga rather than Au in GaAs NW growths. Furthermore, theoretical models [12] that were experimentally

Optical Sensing, Imaging, and Photon Counting: Nanostructured Devices and Applications 2017, edited by Manijeh Razeghi, Oleg Mitrofanov, José Luis Pau Vizcaíno, Chee Hing Tan, Proc. of SPIE Vol. 10353, 103530F · © 2017 SPIE · CCC code: 0277-786X/17/$18 · doi: 10.1117/12.2274007

Downloaded From: https://www.spiedigitallibrary.org/conference-proceedings-of-spie on 10/26/2017 Terms of Use: https://spiedigitallibrary.spie.org/ss/TermsOfUse.aspx

confirmed [13], predicted that Ga-assisted GaAs NWs present a better phase perfection due to Ga droplet partially wets the sidewalls of the NWs during the VLS mechanism. Although, the growth mechanisms of Ga-assisted GaAs NWs on Si have been analyzed as a function of the growth conditions [14], a few studies have addressed the role of parasitic species, comprising GaAs traces and nanocrystals, on the NW growth. Si substrates with pre-lithographed nano-holes along the SiO_x surface layer are commonly used in Ga-assisted MBE to prevent the parasitic growth [7, 8], allowing for the precise positioning of NWs along the substrate surface. However, this procedure requires the use of nanolithography techniques and is not straightforward to CBE due to the thickness of SiO_x (typically 20−30 nm) would not enable the thermal decomposition of metalorganic precursors.

Mechanical manipulation of NWs for their integration in electronics is problematic because of their reduced dimensions, risking to harm the NW body during the assembly process. In this regard, contactless NW manipulation methods using electromagnetic fields –like dielectrophoresis (DEP)– are usually much softer than mechanical methods such as contact transfer printing or tape peeling, often resulting less destructive. Different assembly methods have been developed to manipulate NWs, including fluidic alignment, roll contact printing [15, 16], Langmuir-Blodgett (LB) film deposition technique, drop-casting [17, 18], nano-manipulation [19, 20], and dielectrophoresis [21-26]. Fluidic alignment, roll contact printing transfer, and LB techniques, all offer the ability to align NWs in parallel but do not allow for precise NW placement in functional systems. On the other hand, drop-casting is a low-cost technique but it also requires time-consuming procedures, resulting in very low and stochastic fabrication yields that are limited by the uncontrolled NW concentration in the liquid suspension and also by deposition conditions. The nano-manipulation of NWs is commonly intended by using an atomic force microscopy (AFM) cantilever to interact with the nanostructures by applying lateral forces of the appropriate magnitude. However, the mechanical interaction between the AFM cantilever and the NW can harm the NW structure during the manipulation process; in addition, this technique is limited to the manipulation of a reduced number of NWs at the same time. The assembly of NWs through dielectrophoresis has attracted attention of researchers due to the ability of this technique to precisely position NWs at specific places on a substrate [21-26], making possible the fabrication of NW based applications including field effect transistors (FET) [27, 28], biosensors [29], and other functional electronic devices [30]. Moreover, this approach allows to assemble NWs directly on flexible substrates and at large-areas which is promising for the development of flexible light-emitting diode (LED) displays [31], and transparent flexible nano-electronics [32]. These applications require the accurate control on the number of assembled NWs, as well as, the optimization of the assembling yield. The latter has been extensively reported in different long aspect-ratio nanostructures, showing alignment yields for single Si NWs up to 98.5%/site over an area of 400 mm^2 [33], for InAs NWs up to 70%/site over an area of 0.25 mm^2 [25], and for single wall carbon nanotube (SWCNT) up to 90.0%/site over an area of 0.01 mm^2 [34]. Here, we report a feasible and reproducible dielectrophoretic method to assemble single GaAs NWs on conductive electrodes with an assembling yield above 90%/site, and an alignment yield of 95%. In this regard, we study the dielectrophoretic force exerted over a GaAs NW as a function of key parameters such as voltage amplitude and frequency, analyzing the effects of these parameters on the NW alignment relative to the electric field and the assembly efficiency. This analysis did not exist previously in GaAs NWs, aiding refinements of dielectrophoretic assembly models for different semiconducting NWs [23].

In this work, we optimize the conventional Ga-assisted VLS process by introducing a pioneer “two-steps process” that allows to enhance NW aspect ratio and growth rate, while hindering the nucleation of parasitic species on the growth substrate surface. Then, we analyze the DEP assembling process to align and to trap a controlled number of GaAs NWs between conductive electrodes. Optoelectronic characteristics of single GaAs NW are analyzed to probe the viability of these semiconducting nanostructures as building blocks for photodetecting applications.

2. MATERIALS AND METHODS

2.1 Synthesis of GaAs NWs

GaAs NWs have been grown by Ga-assisted CBE on oxidized Si(111) substrates, using triethylgallium (TEGa), and tertiarybuthylarsine (TBAs) as Ga and As metalorganic precursors, respectively. In this work, we compare two different growth procedures based on the Ga-assisted VLS, called here “one-step” and “two-steps” growths. Prior to each growth, substrates were etched in a 10% HF aqueous solution for 5 min and N_2 blow dried. This first etching step aims to remove the native oxide layer (SiO_x) capping the Si surface whose thickness was about 1.5 nm as determined by spectroscopic ellipsometry. After the above etching, substrates are In-bonded onto a molybdenum sample holder in a hot plate at 200 ºC. Once the substrate is cooled down to room-temperature, it is etched again for 5 min, using the same HF solution, to remove the oxide grown during the bonding stage. Prior to sample introduction in the CBE system under high vacuum

Downloaded From: https://www.spiedigitallibrary.org/conference-proceedings-of-spie on 10/26/2017 Terms of Use: https://spiedigitallibrary.spie.org/ss/TermsOfUse.aspx

conditions, substrates were exposed to the air ambient conditions for 5 min to obtain the final SiO_x thickness of 0.5 nm in a controlled way. This etching procedure results in a thin film of SiO_x with a random distribution of pinholes where Ga droplets can be preferentially formed. A thorough analysis of SiO_x role on the GaAs NWs nucleation was developed by Fontcuberta et al. [35].

The one-step growth procedure and conditions were thoroughly described elsewhere [10]. Briefly, this procedure consists in: i) a substrate annealing for 5 min at a substrate temperature (T_s) of 650 ºC in order to desorb possible remnant adsorbed molecules at the substrate surface (Figure 1(a)); ii) a pre-deposition of 7.5 Ga atomic monolayers (MLs) by opening TEGa valve and at a T_s of 580 ºC, allowing for the Ga droplets formation on the oxidized Si(111) surface, followed by a stabilization stage which allows the rearrangement of Ga droplets during a stabilization time (t_s) of 90 s (TEGa valve is close), leading to the improvement of the droplet size uniformity (Figure 1(b)); iii) finally, both TEGa and TBAs valves are opened at a V/III flux ratio of 0.8, enabling the NW growth at a growth rate (r_g) of around 5.4 μm/h (Figure 1(c)); the r_g was estimated dividing the nanowire length (L_{NW}) determined from SEM images by the total growth time. Furthermore, the NW growth stage was carried out under a substrate rotation of around 5 rpm to ensure a better gas flux uniformity on the substrate surface.

The two-steps growth consists in a "pre-growth" of GaAs NWs carried out during 4 min under the same conditions than those described for the one-step growth method (Figure 1(a-c)). Then, we take the samples out the CBE system and exposure them to the air ambient conditions for one hour to promote the increase of the SiO_x thickness (Figure 1(d)). Thereafter, the samples are transfer to the CBE system and annealed for 5 min at moderate temperatures around T_s = 600 ºC, aiming to desorb surface oxide covering both NW sidewalls and Ga droplet, while preserving the SiO_x layer thickness (Figure 1(e)). Finally, the temperature is lowered down to T_s = 580 ºC and a "re-growth" is carried out for different times by opening both TEGa and TBAs valves, using the same V/III flux ratio of 0.8 (Figure 1(f)).

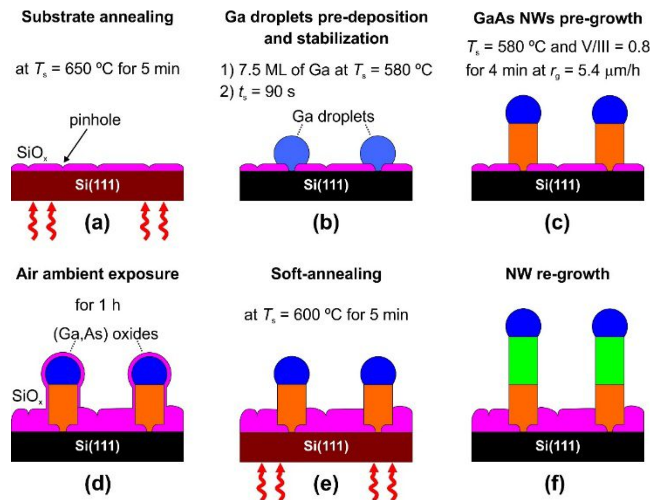

Figure 1. Schematic illustration of the two-steps growth consisting in: (a-c) one-step growth, (d) air ambient exposure, (e) soft-annealing and (f) re-growth.

2.2 DEP Assembly of GaAs NWs

The assembly of GaAs NWs, comprising the integration and alignment of NWs at specific places on a receiver substrate, is carried out by DEP. Ga-assisted VLS growth results in a high-density and random distribution of GaAs NWs vertically aligned with respect to the Si growth substrate. As-grown samples are dipped in an ethanol solvent, and sonicated for a few seconds to remove NWs from the growth substrate. In this regard, two different suspensions are prepared, consisting in GaAs NWs with and without a Ga droplet on top of their tips, aiming to analyze the effect of the Ga droplet on the contact quality formed after the assembling process. The suspension containing GaAs NWs with Ga droplets on their tips will be called suspension A; it was prepared by dipping in 1.5 ml of ethanol a 1 cm^2 sample containing GaAs NWs vertically aligned over a Si(111) substrate, and sonicating it for a few seconds. The sonication step produces the scission of GaAs NWs from the substrate near their base. On the other hand, the suspension containing GaAs NWs without Ga droplets, called here suspension B, was prepared by firstly etching a 1 cm^2 NW sample in a buffered solution of

Downloaded From: https://www.spiedigitallibrary.org/conference-proceedings-of-spie on 10/26/2017 Terms of Use: https://spiedigitallibrary.spie.org/ss/TermsOfUse.aspx

HCl:H_2O (1:9) for 1 min, in order to completely etch Ga droplets, exhibiting then a flat NW front. After Ga droplet etching, NWs were removed from the substrate and transferred to the solvent following the same procedure described for suspension A.

Both Al and AZO electrodes with a thickness of 200 nm are deposited on glass substrates, whose geometry is later defined by photolithography and chemical etching. Electrode gap spacing shorter than the typical NW length is chosen (between 2 and 4 μm) enabling the NWs to bridge the pair of electrodes after their DEP assembly. For the assembly of GaAs NWs between conductive electrodes, a micro-droplet is extracted from the corresponding NW suspension (either A or B) and casted on a substrate with pre-patterned conductive electrodes. An alternating-current (AC) signal with a root-mean-square voltage (V_{rms}) up to 7 V and a frequency (f) between 100 Hz and 1 MHz, is applied between the electrodes, allowing to trap and to align NWs between the electrodes gap due to the dielectrophoretic effect (Figure 2).

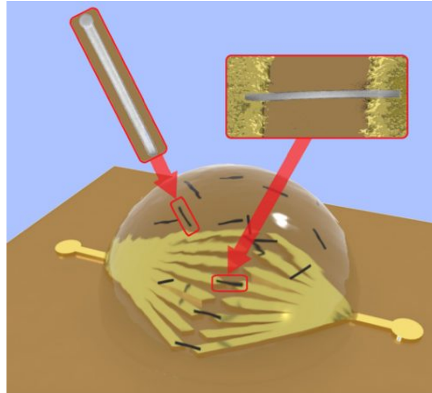

Figure 2. 3D schematic illustration of DEP assembling process of GaAs NWs.

3. THEORETICAL BASICS

The modulus of the dielectrophoretic force (F_{DEP}) exerted on a NW subjected to a non-uniform electric field ($\vec{E}$) in the suspension is given by [21]

$$F_{DEP} = c\,\varepsilon_m \,\mathrm{Re}[f_{cm}]\nabla|E|^2 \qquad (1)$$

where c is the shape-volume factor depending on both the NW radius (r_{NW}) and length (L_{NW}) through the equation

$$c = 1/2\, r_{NW}^2 L_{NW} \qquad (2)$$

for a cylindrical NW; ε_m is the dielectric permittivity of the medium; $\nabla|E|^2$ is proportional to V_{rms}; Re[f_{cm}] is the real part of the Classius-Mossotti factor (f_{cm}) given by

$$f_{cm} = \frac{\varepsilon_p^* - \varepsilon_m^*}{\varepsilon_m^* + L_i\left(\varepsilon_p^* - \varepsilon_m^*\right)} \qquad (3)$$

L_i being the depolarization factor and depends on the relative orientation of the NW respect to $\vec{E}$; ε_p^* and ε_m^* are complex dielectric permittivity of the NW and the medium, respectively, and can be calculated as

$$\varepsilon^* = \varepsilon - j\left(f\sigma/2\pi\right) \qquad (4)$$

where ε is the dielectric permittivity and σ is the electrical conductivity; from Eq. (4), one can conclude that f_{cm} depends on the frequency (f) of the applied AC signal through ε^*

Downloaded From: https://www.spiedigitallibrary.org/conference-proceedings-of-spie on 10/26/2017 Terms of Use: https://spiedigitallibrary.spie.org/ss/TermsOfUse.aspx

4. RESULTS AND DISCUSSION

4.1 Characterization of As-grown GaAs NWs

One-step VLS growth. In a Ga-assisted growth, the formation of Ga droplets on top of the Si substrate surface is necessary to allow the VLS growth of GaAs NWs. Specially in CBE, the preparation of the Si(111) substrate, i.e. the preparation of a thin film of SiO_x, is crucial to enable the thermal decomposition of TEGa molecules on top of the oxidized Si, resulting in Ga droplets randomly distributed along the substrate surface. Aforementioned HF etching procedure of Si wafers results in a thin film of SiO_x with a random distribution of pinholes where Ga droplets can be preferentially formed. A thorough analysis of the SiO_x role on the GaAs NWs nucleation was developed by Fontcuberta et al. [35] The nucleation of Ga droplets was confirmed *in-situ* by RHEED and *ex-situ* by SEM [10].

Since both TEGa and TBAs gas fluxes are opened during the growth step (Figure 1(c)), each droplet becomes supersaturated of As, producing a GaAs solid phase at the droplet/NW interface, and resulting in a GaAs NW underneath the droplet with a hexagonal small footprint as presented in Figure 3(a,b). The analysis carried out *in-situ* by RHEED shows that 90 s after the TBAs was opened, the streaky pattern corresponding to Si(111) substrate surface (not shown) changes to a spotty pattern (Figure 3(c)). RHEED pattern associated to the NWs consists of elongated horizontal lines whose horizontal separation is similar than that observed between vertical bars in the initial streaky pattern of Si, confirming the epitaxial growth of GaAs NWs on the Si(111) substrate. The origin of the horizontal lines can be explained due to the diffraction of the electron beam through a vertically aligned NW, whose small footprint leads to the elongation of the diffracted spot along the horizontal direction. In addition, two different collections of horizontal lines are observed in the NWs RHEED pattern measured along the <1-10> azimuth, labeled as α and β in Figure 3(c), which are associated to reflections of zincblende (ZB) GaAs planes and its 60 degrees' rotational twin, respectively; γ being the specular spot of the incident electron beam. The crystalline structure of these NWs where studied elsewhere by transmission electron microscopy and Raman spectroscopy, confirming the formation of a pure ZB structure and free of rotational twins [13,36].

During the NW growth, other GaAs based species such as traces and nanocrystals (called here parasitic species) can also nucleate along the NWs vicinity (Figure 3(a,b)). The nucleation of these parasitic species was also observed in MBE processes using thick dielectric layers, and was linked to the chemical interaction between the Ga droplets and the dielectric layer [35]. From Figure 3(a) one can conclude that there are two different collections of nanocrystals rotated 60º between each other, whose edges are aligned with the hexagonal based of the NWs, indicating that nanocrystals have nucleated on the Si substrate surface at regions with thinner oxide. The density of parasitic species tends to increase over the growth time which could be an important issue to preserve the initial growth conditions, then, limiting the maximum length of the NWs and hindering their aspect ratio. In this regard, growths carried out at r_g of 5.4 μm/h at conditions described in Figure 1(c) resulted in a polycrystalline layer covering the whole substrate surface for long growth times above 60 min.

The formation of parasitic species was also confirmed by RHEED after 5−6 min of growth, due to the observation of new spots in the difractogram such as titled lines underneath the α and β lines and inter-spots labelled as δ in Figure 3(c). The position of δ-spots between Si RHEED lines, indicates the nucleation of a crystalline structure whose lattice constant is larger than Si (5.431 Å), i.e. GaAs (5.653 Å).

During VLS growth, the parasitic species act as a trap of Ga and As atoms, reducing their effective incorporation to the droplet/NW interface, leading to the reduction of the Ga droplet size. Since the NW diameter is affected by the size of the Ga droplet, its reduction directly reduces the NW diameter, resulting in a tapering effect clearly observed in Figure 3(b). Furthermore, if the effective incorporation of Ga to the droplet is not sufficient, the droplet can be completely consumed by the VLS growth, interrupting the longitudinal growth of the NW. In that respect, GaAs NWs with lengths up to 3 μm were obtained [10]. In addition, the axial growth of the NW can be promoted specially at those regions near the NW based which can be an additional factor contributing to the tapering effect observed in Figure 3(b).

Downloaded From: https://www.spiedigitallibrary.org/conference-proceedings-of-spie on 10/26/2017 Terms of Use: https://spiedigitallibrary.spie.org/ss/TermsOfUse.aspx

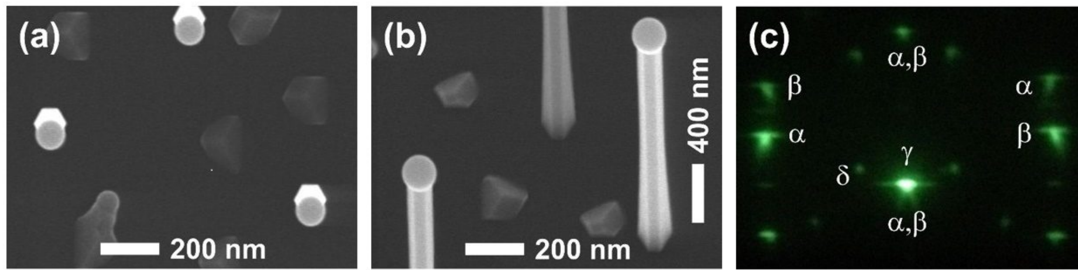

Figure 3. SEM images of GaAs NWs grown by one-step growth taken at (a) 0º, and (b) 30º with respect to the substrate normal direction; (c) corresponding RHEED diffractogram.

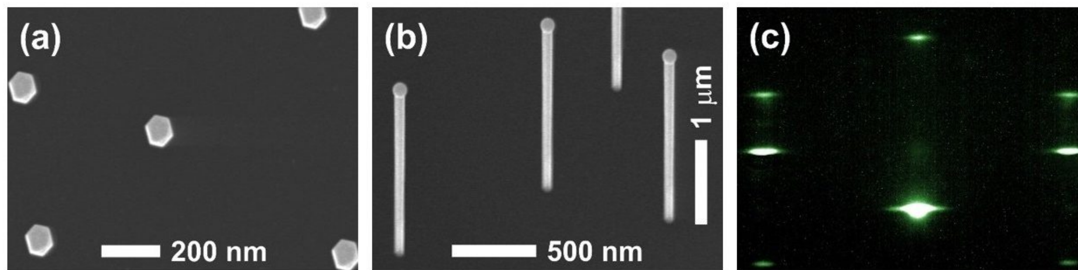

Figure 4. SEM images of GaAs NWs grown by two-steps growth taken at (a) 0º, and (b) 30º with respect to the substrate normal direction; (c) corresponding RHEED diffractogram.

Two-steps VLS growth. In two-steps growth, the scenario is totally different with respect to the one-step growth. As aforementioned in the experimental section, the two-steps growth consists in a first pre-growth carried out during 4 min under the same conditions described for the one-step growth. This time allows for the growth of NWs while preserving the formation of parasitic species, comprising both traces and nanocrystals; thereafter the pre-growth (Figure 1(c)), samples are exposure to the ambient air for 1 hour in order to increase the thickness of the SiO_x layer (Figure 1(d)). This step is crucial to prevent the formation of parasitic species during the re-growth as it will show later on. The re-growth was then carried out using the same conditions than those utilized in the pre-growth. Figure 4(a,b) show SEM images of resulting NWs with a higher aspect ratio and growth rates than those obtained under one-step growth conditions. This result can be explained due to the reduction of the parasitic species under two-steps growth conditions preserves the VLS conditions at the catalyst, leading to the growth of NWs with better aspect ratio, higher growth rate, while observing less tapering effect (Figure 4(a,b)).

The density of NWs was also increased in two-steps growth conditions, showing values about 5.31 μm^{-2} (Figure 4(a)) which are therefore higher than in the one-step growth (3.18 μm^{-2}) estimated from Figure 3(a). From Figure 4(a,b) one can also conclude that the nucleation of parasitic species was totally inhibited. Figure 4(c) presents the characteristic RHEED diffractogram under the <1-10> azimuth, observed during the whole growth under two-steps conditions; as mentioned horizontal lines correspond to the NWs, whereas there were not evidences of inter-spots neither lines underneath the ZB lines which confirm the absence of parasitic species. From these results, RHEED was probed to be a precise tool to determine the formation of different species during the NW growth.

Downloaded From: https://www.spiedigitallibrary.org/conference-proceedings-of-spie on 10/26/2017 Terms of Use: https://spiedigitallibrary.spie.org/ss/TermsOfUse.aspx

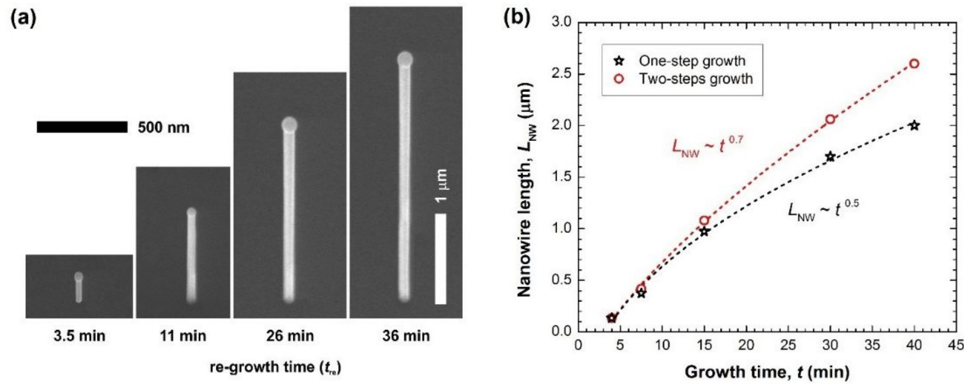

Figure 5. (a) SEM images of GaAs NWs grown under two-steps growth for different t_{re}; (b) L_{NW} vs t for GaAs NWs grown by one-step (black stars) and two-steps (red circles) growths.

GaAs NWs were grown for different re-growth times (t_{re}) ranged between 3.5, 11, 26, and 36 min after a pre-growth time (t_{pre}) of 4 min, resulting in a total growth time ($t = t_{pre} + t_{re}$) of 7.5, 15, 30, and 40 min, respectively. In Figure 5(a), each NW image corresponds to the average NW found for every sample, being representative of the observed NW population. As SEM images were taken at 30º away from the substrate surface normal direction, the apparent vertical dimensions are reduced by a factor of sin 30º = 0.5; so the real scale has to be multiplied by a factor of 2 in order to estimate the L_{NW} directly from Figure 5(a). Figure 5(b) represents the dependence of L_{NW} obtained from SEM images of GaAs NWs grown under one-step (black stars) and two-steps (red circles) growths, as a function of the growth time. From that figure, one can observe that L_{NW} depends on t following a sublinear power law, $L_{NW} \sim t^{x}$, where x is 0.5 and 0.7 in the case of one-step and two-steps growths, respectively. In that respect, the two-steps growth improves the growth rate of the NWs mainly due to two factors, involving lower NW diameters and a drastically decrease of the parasitic species surrounding the NWs.

4.2 GaAs NWs Assembly as a Function of DEP Conditions

The assembly efficiency of the DEP process has been analyzed as a function of different DEP conditions, such as V_{rms} and f values of the applied electric signal. In that respect, F_{DEP} exerted on NWs has been calculated as a function of both V_{rms} and f, assuming GaAs NWs with dimensions of r_{NW} = 50 nm and a L_{NW} = 5 μm with electrical properties given by $\varepsilon_p = 10.89\varepsilon_0$, and σ_p = 6000 S/m, suspended in an ethanol medium ($\varepsilon_m = 24.3\varepsilon_0$ and $\sigma_m = 10^{-5}$ S/m). Calculated F_{DEP} as a function of the AC frequency using Eq. (1) –assuming a NW initially aligned to the electric field (L_i = 0), vertically placed at 10 μm from the electrodes gap, while applying a V_{rms} = 7 V– is shown in Figure 6(a); a typical low-pass response can be observed, including three different regions. After the initial constant force region for f < 100 Hz, a further decrease is observed (as $F_{DEP} \sim 1/f^2$) when increasing the applied AC frequency. Finally, F_{DEP} remains constant at a reduced value for frequency values larger than 30 MHz. At a first sight, it could be deduced from this figure that low frequencies should be better to assemble GaAs NW due to the large force values achieved in this region, but experiments show the opposite result. Ethanol electrolysis observed at low frequencies repels the NW away from the electrodes gap, hindering NW alignment.

DEP assembly vs AC Frequency. To evaluate the effect of the frequency on NWs assembly mechanism, we carried out series of experiments consisting in DEP processes developed by using f values up to 1 MHz. After DEP process, samples are observed by SEM imaging as shown in Figure 6(b–d). The successful trapping of GaAs NWs was observed only for f values above 10 kHz involving F_{DEP} in the pN and nN ranges –as it is highlighted in Figure 6(a)– called here assembly region; in the assembly region, NWs can reach a better alignment with the electric field lines because the NW assembly process is carried out under lower F_{DEP} values, resulting in a slower and softer process than for low frequency values. In this regard, the NW assembly yield was studied using frequency conditions corresponding to the assembly region between 10 kHz and 1 MHz. The effect of a softer alignment procedure is shown in Figure 6(b–d) where the assembly angle –defined as the final angle between NWs and the electric field lines normal to both electrodes– is progressively reduced as the DEP frequency is increased, demonstrating the improvement of the NW alignment when increasing f between 10 kHz and 1MHz. Under frequency conditions ranging between 10 kHz and 1 MHz, we observed an alignment yield above 95%, comprising NW alignments below 5º with respect to the alignment direction.

Downloaded From: https://www.spiedigitallibrary.org/conference-proceedings-of-spie on 10/26/2017 Terms of Use: https://spiedigitallibrary.spie.org/ss/TermsOfUse.aspx

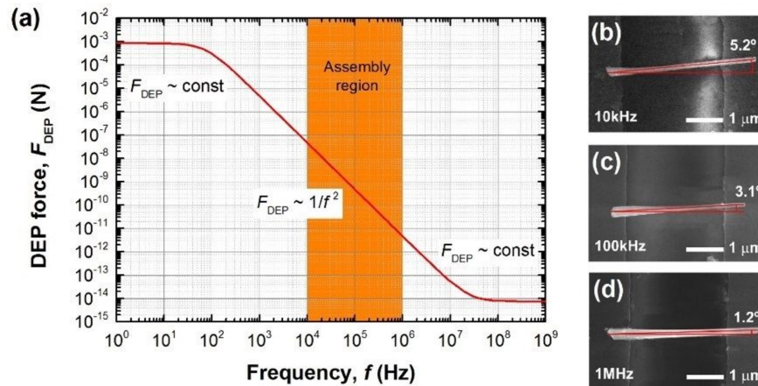

Figure 6. (a) F_{DEP} exerted on a GaAs NW dipped in ethanol as a function of AC frequency; (b‒c) SEM images of GaAs NWs alignment by DEP using different AC frequencies.

DEP Assembly vs AC voltage. F_{DEP} applied to a GaAs NW as a function of the applied V_{rms} value can also be calculated using Eq. (1). Considering a typical situation involving a GaAs NW initially aligned along the electric field (L_i = 0), vertically placed at 10 μm from the electrodes gap, using an AC frequency of f = 100 kHz, the calculated F_{DEP} for V_{rms} values up to 7 V is plotted in Figure 7(a). That figure shows how GaAs NWs are subjected to a F_{DEP} whose magnitude increases as the square of the applied V_{rms} value; the above behavior is also indicated by the fitted line to calculated data, reaching values close to 0.5 nN for V_{rms} = 7 V. To probe the validity of the above calculations, DEP experiments were also carried out using wide-sized electrodes (100 μm) separated by a 2 μm gap, allowing for the assembly of multiple NWs interconnecting both electrodes (see inset of Figure 7(b)). Several V_{rms} values were used in different DEP processes, whose resulting SEM images are also shown in Figure 7(b). The duration of the DEP process is limited by the evaporation of the droplet, lasting typically around 30 s. From SEM images shown in Figure 7(b) it is noticeable that a V_{rms} value of 4.24 V is not enough to trap any GaAs NW along the electrode length; the above V_{rms} value produces F_{DEP} = 0.15 nN, which is not sufficiently high to overcome the drag force in the fluid. For larger V_{rms} values, such as 5.66 V and 7.07 V, F_{DEP} is large enough to successfully trap NWs between the electrodes gap, obtaining NW densities of 0.02 and 0.08 NW/μm. The observed increase on the assembled NW density with increasing V_{rms} values is in good agreement to the trend predicted in Figure 7(a).

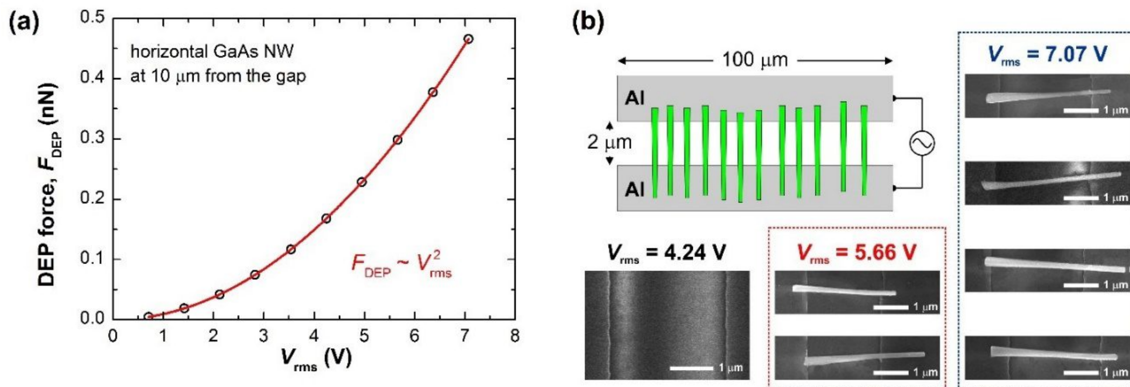

Figure 7. (a) F_{DEP} exerted on a GaAs NW as a function of the AC voltage (V_{rms}). Calculated data (circles) and fitting (line) are shown; (b) SEM images of three DEP experiments carried out at different V_{rms} values and schematic of the electrode geometry.

DEP Assembly vs NW-to-electrodes Gap Distance. The F_{DEP} exerted on a GaAs NW has been also calculated as a function of the distance between the NW and the electrodes gap. DEP force calculations have been performed using previously obtained optimum values of f = 100 kHz and V_{rms} = 7.07 V, assuming a NW initially aligned along the electric field (L_i = 0) and using 2 μm of electrode spacing. For the sake of simplicity, the distance between the NW and the electrodes is calculated along the sample normal direction (z axis) such as represented in the left vertical axis of Figure 8. This figure represents the F_{DEP} calculated amplitude values using constant magnitude arrows to represent its direction;

Downloaded From: https://www.spiedigitallibrary.org/conference-proceedings-of-spie on 10/26/2017 Terms of Use: https://spiedigitallibrary.spie.org/ss/TermsOfUse.aspx

the figure also includes a colour scale to represent the F_{DEP} magnitude, which is very sensitive to the distance. The applied F_{DEP}, as seen in this figure, is always pointing towards the electrode gap, allowing for NW trapping.

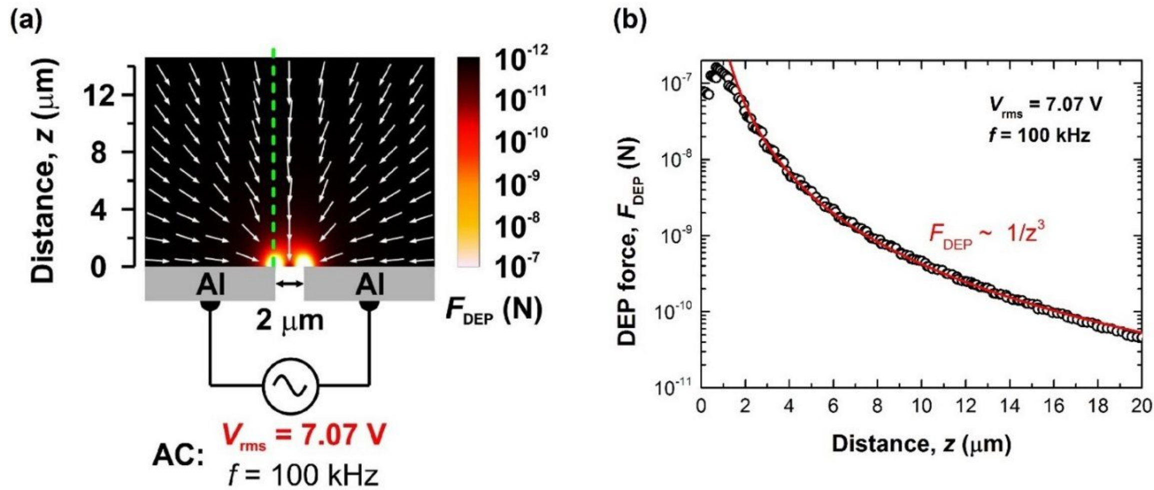

Figure 8. Calculation of F_{DEP} field as a function of distance. (a) Constant magnitude arrows are used to represent F_{DEP} direction; (b) calculated F_{DEP} amplitude versus distance along the green dotted line represented in (a).

The F_{DEP} dependence on the distance (z) along a vertical line starting on one electrode corner (dotted green line drawn in Figure 8(a)), is plotted in Figure 8(b). A fast decrease of F_{DEP} as z increases can be observed in that plot, following an inverse power law (z^{-3}) for distances larger than the electrode separation. Pethig et al. estimated that producing a significant F_{DEP} requires $\nabla|E|^2$ values in the range of 10^{-5} $V^2 \cdot \mu m^{-3}$ or even larger. Our calculations produce F_{DEP} in the pN range, while the above threshold value is reached at 30 μm, indicating NWs could be successfully trapped at distances up to 30 μm away from the electrodes.

DEP assembly of GaAs W and W/O droplet. Using the previously optimized procedure to align between conductive electrodes, we have used DEP to fabricate single NW based photodetectors using two different collections of NWs, with and without Ga droplet on top of the NW, as described in the experimental setup section. Separate but identical procedures were applied to align NWs W or W/O the final droplet, as shown in Figure 9. A micro-droplet of each suspension (4 μl) was deposited on top of a receiver substrate with electrodes, previously defined by optical lithography and lift-off. An AC signal is then applied between those electrodes using the optimized DEP conditions (V_{rms} = 5.66 V, f = 100 kHz) to promote the assembly of a single NW between electrodes. As the DEP force is weighted by the total material volume (see Eq. (1)), the presence of a small volume Ga droplet –even with a different dielectric constant– at the end of the GaAs NW is not expected to significantly change the DEP process. Images of the NW assembled on both contacts are seen in Figure 9 for NWs W and W/O Ga droplet. At the bottom left image of Figure 9(a), it can be observed that the Ga droplet is alloyed with the electrode after NW alignment. This is a consequence of the low melting point of Ga and the heat resulting from the application of an AC bias between coplanar contacts in a liquid medium that leads to a local increase of the temperature even for solvents with moderate ionic strengths.

Downloaded From: https://www.spiedigitallibrary.org/conference-proceedings-of-spie on 10/26/2017 Terms of Use: https://spiedigitallibrary.spie.org/ss/TermsOfUse.aspx

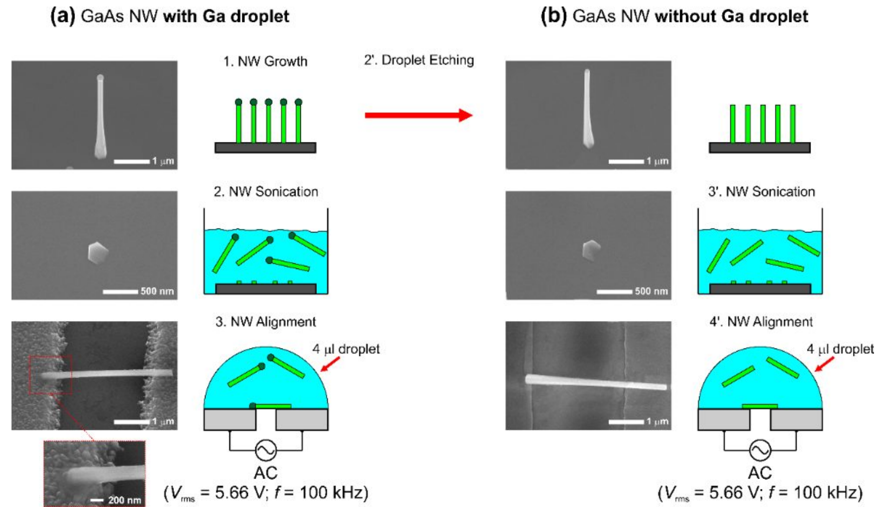

Figure 9. Procedure to obtain GaAs NWs aligned between conductive electrodes. (a) Ga-terminated NWs and (b) NWs W/O the final Ga droplet. Images of the corresponding NWs after growth (lateral and top views) and after alignment are shown.

4.3 Photoresponse of Single GaAs NW based PDs

Figure 10 shows the I-V characteristics of the device based on a single NW without Ga droplet. A very low conductivity can be observed in this device, exhibiting low currents in the pA range. The GaAs/Al or GaAs/AZO contacts could act as Schottky barriers in these devices, giving rise to the formation of two opposite Schottky diodes, as represented in the equivalent circuit of Figure 10. Moreover, these devices do not show any sensitivity to the visible light exposure, as observed when comparing both curves, with and without visible light illumination.

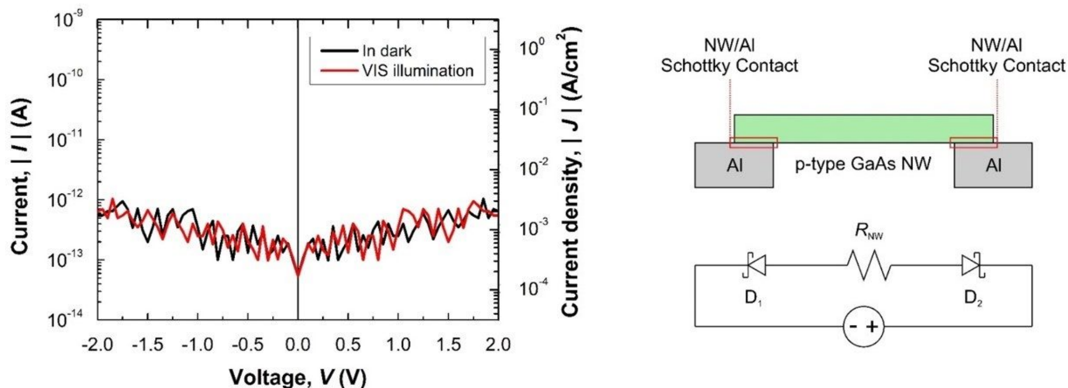

Figure 10. I-V characteristics of the device fabricated using a non Ga-terminated NW under dark conditions and visible illumination (left). A schematic picture and the equivalent circuit of the device (right) are also included.

On the other hand, devices based on Ga droplet-terminated NWs show asymmetric and diode like I-V curves, as shown in Figure 11. Probably, the formation of a low contact resistance at the AZO electrode-Ga droplet-NW end contact is responsible for this behavior; this ohmic contact is built thanks to the formation of the droplet during the VLS growth and strongly enhances the conduction of the device.

Finally, the photo-responsivity of these devices was measured, resulting in an evident photosensitivity to the visible light when the device is forward biased. A clear increase of the forward current –close to two orders of magnitude– can be observed in Figure 11 As the device current in that bias range is limited by the series resistance of the device, the

Downloaded From: https://www.spiedigitallibrary.org/conference-proceedings-of-spie on 10/26/2017 Terms of Use: https://spiedigitallibrary.spie.org/ss/TermsOfUse.aspx

observed increase is attributed to a reduction of the series resistance under illumination. On the other hand, the device does not show any evidence of photo-generated current in the reverse bias region, where the device current is limited by the transport through the potential barrier at the contact formed by DEP between the NW and the AZO layer.

It is well known that GaAs surface, even covered with a native oxide, exhibits a large density of surface states located inside the bandgap, giving rise to an important band bending near the surface (Fermi level pinning) and to a carrier depleted region. When GaAs NWs are not passivated at the NW sidewalls (as it is for the NWs of this work), the NW body can be partly or fully depleted due to both, the Fermi-level pinning effect and the reduced NW diameter; this effect can reduce the effective NW section for conduction, and thus, the electrical conductance. Under illumination conditions, electron-hole pairs are created by photon absorption, increasing the carrier density in the NW body; band-bending is then reduced and also the depletion width near the NW surface, increasing the NW effective section for conduction. This effect, also found in other semiconductor NW technologies, explains the observed reduction of the device series resistance under illumination and the corresponding increase of the forward current [21].

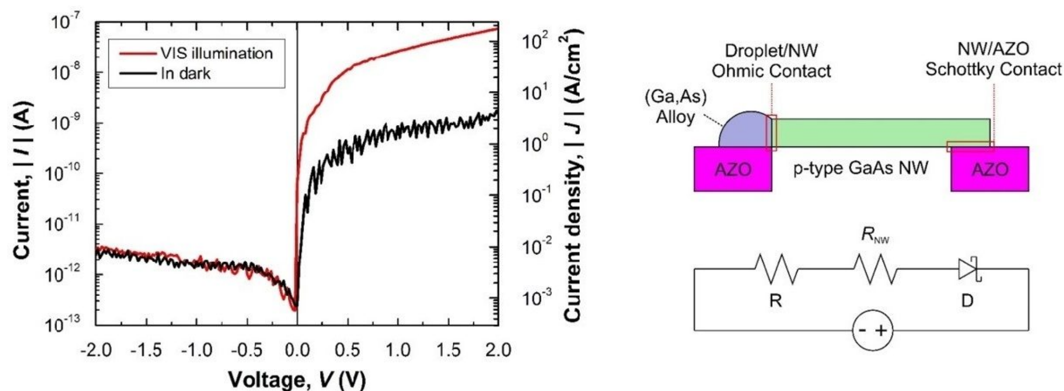

Figure 11. I-V characteristics of the device fabricated using a Ga-terminated NW under dark conditions and visible illumination (left). A schematic picture and the equivalent circuit of the device (right) are also included.

5. CONCLUSIONS

In this work, we have compared morphological characteristics of GaAs NWs grown by CBE through “one-step” and “two-steps” growth methods. From this comparison, one can conclude that adding an intermediate oxidation step between a pre-growth and a re-growth, i.e. a two-steps growth, strongly reduce the nucleation of parasitic species on the growth substrate, which improve the aspect ratio of resulting NWs, by reducing the tapering effect. This method also increases the NW growth rate, which will benefit the integration of resulting NWs in electronic circuits.

The assembly of CBE GaAs NWs has been investigated by DEP, being a pioneer technique for this kind of NWs. The influence of DEP parameters, such as AC frequency and amplitude, as well as the role of the electrodes material and the catalyst on top of the NW has been analyzed. From these studies, one can conclude that amplitude and frequency values of the applied AC signal are critical parameters to control the number of assembled NWs; V_{rms} values in the 4 to 7 V range with frequencies in the 10 kHz to 1MHz range have been successfully used to align GaAs NWs with an assembly yield above 90% and an alignment yield above 95% (considering only those NWs misaligned up to 5º with respect to the alignment direction). The optimization of these DEP parameters, comprising V_{rms} and AC frequency, allowed us to fabricate devices based on a single GaAs NW with and without the final Ga droplet. These results demonstrated the use of DEP as a promising, low-cost and ease of developing technique for the controlled, feasible, and reproducible assembly of elongated nanostructures at specific places, allowing the fabrication of complex arrays and 2D/3D monolithic structures for multiple advanced optoelectronic applications. I-V characteristics of single GaAs NWs with and without the final Ga droplet have also been measured; while devices based on a GaAs NW without Ga droplet presented noisy currents in the pA range, both in dark and under visible illumination, devices based on Ga droplet-terminated GaAs NWs exhibited asymmetrical diode-like I-V curves in the pA range with an increased forward current under visible illumination. The high photoresponse demonstrated the viability to use single GaAs NWs based devices as photodetectors in the visible range.

Downloaded From: https://www.spiedigitallibrary.org/conference-proceedings-of-spie on 10/26/2017 Terms of Use: https://spiedigitallibrary.spie.org/ss/TermsOfUse.aspx

6. ACKNOWLEDGEMENTS

N. López acknowledges support of the European Commission by Marie Curie International Incoming Fellowship PIIF-GA-2012-326579. The authors also acknowledge the support from MINECO under TEC2013-48350-R and TEC2016-78433-R projects.

*Corresponding author: basilio.javier.garcia@uam.es

7. REFERENCES

[1] Krogstrup, P., Jørgensen, H. I., Heiss, M., Demichel, O., Holm, J. V., Aagesen, M., Nygard, J. and i Morral, A. F., "Single-nanowire solar cells beyond the Shockley-Queisser limit," Nature Photonics 7(4), 306-310 (2013).
[2] Wang, H., "High gain single GaAs nanowire photodetector," Applied Physics Letters 103(9), 093101-1-093101-4 (2013).
[3] Björk, M., Ohlsson, B., Thelander, C., Persson, A., Deppert, K., Wallenberg, L and Samuelson, L., "Nanowire resonant tunneling diodes," Applied Physics Letters 81(23), 4458-4460 (2002).
[4] Kasai, S. and Hasegawa, H., "A single electron binary-decision-diagram quantum logic circuit based on Schottky wrap gate control of a GaAs nanowire hexagon," IEEE Electron Device Letters 23(8), 446-448 (2002).
[5] Heinrich, J., Huggenberger, A., Heindel, T., Reitzenstein, S., Höfling, S., Worschech, L and Forchel, A., "Single photon emission from positioned GaAs/AlGaAs photonic nanowires," Applied Physics Letters 96(21), 211117-1-211117-3 (2010).
[6] Wagner, R. S. and Ellis, W. C., "Vapor-liquid-solid mechanism of single crystal growth," Applied Physics Letters 4(5), 89-90 (1964).
[7] Plissard, S., Larrieu, G., Wallart, X and Caroff, P., "High yield of self-catalyzed GaAs nanowire arrays grown on silicon via gallium droplet positioning," Nanotechnology 22(27), 275602-1-275602-7 (2011).
[8] Munshi, A. M., Dheeraj, D. L., Fauske, V. T., Kim, D.-C., Huh, J., Reinertsen, J. F., Ahtapodov, L., Lee, K., Heidari, B. and Van Helvoort, A., "Position-Controlled Uniform GaAs Nanowires on Silicon using Nanoimprint Lithography," Nano letters 14(2), 960-966 (2014).
[9] Persson, A., Ohlsson, B., Jeppesen S. and Samuelson, L., "Growth mechanisms for GaAs nanowires grown in CBE," Journal of Crystal Growth 272(1), 167-174 (2004).
[10] García Núñez, C., Braña, A. F., López, N. and García, B. J., "GaAs nanowires grown by Ga-assisted chemical beam epitaxy: Substrate preparation and growth kinetics," Journal of Crystal Growth 430, 108-115 (2015).
[11] Perea, D. E., Allen, J. E., May, S. J., Wessels, B. W., Seidman, D. N. and Lauhon, L. J., "Three-dimensional nanoscale composition mapping of semiconductor nanowires," Nano letters 6(2), 181-185 (2006).
[12] Dubrovskii, V., Cirlin, G., Sibirev, N., Jabeen, F., Harmand, J., Werner, P., "New Mode of Vapor-Liquid-Solid Nanowire Growth," Nano letters 11(3), 1247-1253 (2011).
[13] García Núñez, C., Braña, A. F., Pau, J. L., Ghita, D., García, B. J., Shen, G., Wilbert, D. S., Kim, S. M. and Kung, P., "Pure zincblende GaAs nanowires grown by Ga-assisted chemical beam epitaxy," Journal of Crystal Growth 372, 205-212 (2013).
[14] Cirlin, G., Dubrovskii, V., Samsonenko, Y. B., Bouravleuv, A., Durose, K., Proskuryakov, Y. Y., Mendes, B., Bowen, L., Kaliteevski, M. and Abram, R., "Self-catalyzed, pure zincblende GaAs nanowires grown on Si(111) by molecular beam epitaxy," Physical Review B 82(3), 035302-1-035302-6 (2010).
[15] Bai, S., Wu, W., Qin, Y., Cui, N., Bayerl, D. J., & Wang, X., "High-Performance Integrated ZnO Nanowire UV Sensors on Rigid and Flexible Substrates," Advanced Functional Materials, 21(23), 4464-4469 (2011).
[16] Chang, Y.-K. and Hong, F. C.-N., "The fabrication of ZnO nanowire field-effect transistors by roll-transfer printing," Nanotechnology 20(19), 195302-1-195302-6 (2009).
[17] Yao, H. B., Ge, J., Wang, C. F., Wang, X., Hu, W., Zheng, Z. J., Ni, Y. and Yu, S. H., "A flexible and highly pressure-sensitive graphene–polyurethane sponge based on fractured microstructure design," Advanced Materials 25(46), 6692-6698 (2013).
[18] Ramgir, N., Sen, S., Kaur, M., Mishra, S. K., Rikka, V., Choukikar, R., & Muthe, K., "Investigation of SnO2 nanowire based gas sensors," Asian Journal of Physics, 19, 273-278 (2010).

Downloaded From: https://www.spiedigitallibrary.org/conference-proceedings-of-spie on 10/26/2017 Terms of Use: https://spiedigitallibrary.spie.org/ss/TermsOfUse.aspx

[19] Avouris, P., Hertel, T., Martel, R., Schmidt, T., Shea, H. R. and Walkup, R. E., "Carbon nanotubes: nanomechanics, manipulation, and electronic devices," Applied Surface Science 141(3), 201-209 (1999).
[20] Peng, Y., Luxmoore, I., Forster, M., Cullis, A. and Inkson, B., "Nanomanipulation and electrical behaviour of a single gold nanowire using in-situ SEM-FIB-nanomanipulators," Journal of Physics: Conference Series 126(1), 012031 (2008).
[21] García Núñez, C., García Marín, A., Nanterne, P., Piqueras, J., Kung, P. and Pau, J. L., "Conducting properties of nearly depleted ZnO nanowire UV sensors fabricated by dielectrophoresis," Nanotechnology 24(41), 415702-1-415702-10 (2013).
[22] Javey, A., Guo, J., Wang, Q., Lundstrom, M. and Dai, H., "Ballistic carbon nanotube field-effect transistors," Nature 424(6949), 654-657 (2003).
[23] Min, K. W., Kim, Y. K., Shin, G., Jang, S., Han, M., Huh, J., Kim, G. T. and Ha, J. S., "White-Light Emitting Diode Array of p+-Si/Aligned n-SnO2 Nanowires Heterojunctions," Advanced Functional Materials 21(1), 119-124 (2011).
[24] Javey, A., Kim, H., Brink, M., Wang, Q., Ural, A., Guo, J., McIntyre, P., McEuen, P., Lundstrom, M and Dai, H., "High-κ dielectrics for advanced carbon-nanotube transistors and logic gates," Nature materials 1(4), 241-246 (2002).
[25] Small, W. R., "Inkjet Printing of Transparent, Electrically Conducting Single-Walled Carbon-Nanotube Composites," Small 3(9), 1500-1503 (2007).
[26] Joselevich, E. and Lieber, C. M., "Vectorial growth of metallic and semiconducting single-wall carbon nanotubes," Nano Letters 2(10), 1137-1141 (2002).
[27] Chen, Y.-M., He, S.-M., Huang, C.-H., Huang, C.-C., Shih, W.-P., Chu, C.-L., Kong, J., Li, J. and Su, C.-Y., "Ultra-large suspended graphene as a highly elastic membrane for capacitive pressure sensors," Nanoscale 8(6), 3555-3564 (2016).
[28] Tian, H., Shu, Y., Wang, X.-F., Mohammad, M. A., Bie, Z., Xie, Q.-Y., Li, C., Mi, W.-T., Yang, Y., Ren and T.-L., "A graphene-based resistive pressure sensor with record-high sensitivity in a wide pressure range," Scientific Reports 5, 8603(2015).
[29] Metzger, C., Fleisch, E., Meyer, J., Dansachmüller, M., Graz, I., Kaltenbrunner, M., Keplinger, C., Schwödiauer, R. and Bauer, S., "Flexible-foam-based capacitive sensor arrays for object detection at low cost," Applied Physics Letters 92(1), 013506 (2008).
[30] Shirinov, A. and Schomburg, W., "Pressure sensor from a PVDF film," Sensors and Actuators A: Physical 142(1), 48-55 (2008).
[31] Kim, K., Moon, T., Lee, M., Kang, J., Jeon, Y. and Kim, S., "Light-emitting diodes composed of n-ZnO and p-Si nanowires constructed on plastic substrates by dielectrophoresis," Solid State Sciences 13(9), 1735-1739 (2011).
[32] Ju, S., Facchetti, A., Xuan, Y., Liu, J., Ishikawa, F., Ye, P., Zhou, C., Marks, T. J. and Janes, D. B., "Fabrication of fully transparent nanowire transistors for transparent and flexible electronics," Nature nanotechnology 2(6), 378-384 (2007).
[33] Freer, E. M., Grachev, O., Duan, X., Martin, S. and Stumbo, D. P., "High-yield self-limiting single-nanowire assembly with dielectrophoresis," Nature nanotechnology 5(7), 525-530 (2010).
[34] Fan, Z., Ho, J. C., Jacobson, Z. A., Razavi, H and Javey, A., "Large-scale, heterogeneous integration of nanowire arrays for image sensor circuitry," Proceedings of the National Academy of Sciences 105(32), 11066-11070 (2008).
[35] Fontcuberta i Morral, A., Colombo, C., Abstreiter, G., Arbiol and J., Morante, J., "Nucleation mechanism of gallium-assisted molecular beam epitaxy growth of gallium arsenide nanowires," Applied Physics Letters 92(6), 063112-1-063112-3 (2008).
[36] García Núñez, C., Braña, A. F., Pau, J. L., Ghita, D., García, B. J., Shen, G., Wilbert, D. S., Kim, S. M. and Kung, P., "Surface optical phonons in GaAs nanowires grown by Ga-assisted chemical beam epitaxy," Journal of Applied Physics 115(3), 034307 (2014).

Downloaded From: https://www.spiedigitallibrary.org/conference-proceedings-of-spie on 10/26/2017 Terms of Use: https://spiedigitallibrary.spie.org/ss/TermsOfUse.aspx